Signal-Based H_8 Longitudinal Controller Design for the Flying-V Aircraft

Pedroso, Beatriz; Pollack, Tijmen; Theodoulis, Spilios

DOI
10.1016/j.ifacol.2025.10.083

Publication date
2025

Document Version
Final published version

Published in
IFAC-PapersOnline

Citation (APA)
Pedroso, B., Pollack, T., & Theodoulis, S. (2025). Signal-Based H_8 Longitudinal Controller Design for the Flying-V Aircraft. *IFAC-PapersOnline*, *59*(16), 80-85. https://doi.org/10.1016/j.ifacol.2025.10.083

Available online at www.sciencedirect.com

ScienceDirect

IFAC PapersOnline CONFERENCE PAPER ARCHIVE

IFAC PapersOnLine 59-16 (2025) 80–85

Signal-Based $\mathcal{H}_\infty$ Longitudinal Controller Design for the Flying-V Aircraft

Beatriz Pedroso * **Tijmen Pollack** * **Spilios Theodoulis** *

* *Faculty of Aerospace Engineering, Delft University of Technology, Delft, 2629HS, The Netherlands*

Abstract:
Flight control system design for the Flying-V has been an active research area. However, despite the strengths of $\mathcal{H}_\infty$ control, this framework has not yet been considered for the system design. Therefore, this study details the synthesis of a longitudinal control law using the robust control signal-based $\mathcal{H}_\infty$ framework. The trimming procedure used to obtain operating points and linearized flight dynamics is explained, followed by a description of the design requirements which are systematically converted into hard constraints for synthesis. A structured controller design is conducted and the resulting system is evaluated in terms of performance and robustness in linear and nonlinear settings. Results indicate effective disturbance and noise rejection, stability under parametric uncertainties, Level 1 handling qualities predictions, and adequate performance. The C* control law effectiveness paves the way for future enhancements in gain-scheduled robust controllers for the Flying-V and for the extension to lateral-directional designs.

Keywords: Robust control, Signal-based $\mathcal{H}_\infty$ synthesis, Flight control, $\mathcal{H}_\infty$ Optimization, Linearized models, Robust stability, Sustainable aviation, Flying wings.

1. INTRODUCTION

Commercial aviation has experienced a rising demand in recent years. The Flying-V aircraft is introduced as a promising concept that seeks to mitigate the industry's environmental impact. Preliminary assessments by Benad and Vos (2022) suggest that the Flying-V could achieve a 20% lower fuel burn when compared to the state-of-the-art reference aircraft performing the same mission. However, its unconventional shape and layout pose unique challenges in terms of stability and control, necessitating the development of advanced control systems.

Flight control system design for the Flying-V concept aircraft has been an active field in recent years with design methods focusing mainly on nonlinear approaches, namely Incremental Nonlinear Dynamic Inversion (INDI) (Stougie et al., 2024; van Overeem et al., 2023) and adaptive INDI (Atmaca and Kampen, 2025). Although these techniques aim to alleviate the process of gain scheduling, they provide no robustness guarantees in the design phase and they rely on specific structural assumptions. On the contrary, $\mathcal{H}_\infty$ control is a systematic framework that explicitly addresses robustness and performance specifications in the presence of plant model uncertainties and which does not require a predefined controller structure. The $\mathcal{H}_\infty$ control problem solutions obtained via Algebraic Ricatti Equations (Doyle et al., 1988) and Linear Matrix Inequalities (Gahinet and Apkarian, 1994) result in full-order unstructured controllers. Nevertheless, although these resulting controllers are theoretically optimal, these high-order structures might be impractical for implementation in industry due to hardware and software constraints and lack of transparency. To address this limitation, model order reduction techniques can be used to simplify the controllers while retaining the most dominant dynamics. Additionally, reducing the controller's order can also help identifying a simpler and more practical structure that is suitable for industry applications. In light of this, tools for structured $\mathcal{H}_\infty$ synthesis were recently developed. These leverage the investigations conducted on non-smooth optimizers (Apkarian and Noll, 2006) to directly tune single or multiple loop control architecture, using an efficient and parallel computing-aided optimization.

Multivariable robust control is foundational to systematic tuning of control laws that are widely used in industry. However, in spite of its strengths, $\mathcal{H}_\infty$ control has not yet been applied to the Flying-V. Therefore, this research addresses this gap by proposing a systematic design and tuning of a longitudinal flight control system tailored for the Flying-V aircraft. A C* longitudinal control law is implemented which is tuned within the signal-based $\mathcal{H}_\infty$ robust control framework. The suggested solution guarantees robustness against disturbances, measurement noise, and uncertainties in the model while ensuring performance and compliance with Level 1 handling qualities (HQ). Moreover, the imposed controller structure is the result of a preliminary unstructured synthesis and of a subsequent model reduction analysis.

This paper is structured as follows: Section 2 presents the local linearized dynamics, Section 3 discusses the C* parameter and the controller design requirements, structure, synthesis methodology and results, and lastly, Section 4 examines the flight control performance and robustness for the nominal and uncertain scenarios in linear and nonlinear settings, via stability margins, HQ, and nonlinear simulations assessments.

10.1016/j.ifacol.2025.10.083

2. FLYING-V MODEL DESCRIPTIONS

A 6 degrees of freedom (DoF) Flying-V model is implemented in MATLAB ®/Simulink ® in a tensor-based formulation. Tensors hold the physical characteristics regardless of the coordinate system. This generalizes the equations of motion (EoM), allowing for subsequent projection into any coordinate system (Zipfel, 2007).

The trimming procedure is the first step towards linearization of the flight dynamics. It involves a (usually numerical) method which calculates the equilibrium points around an imposed condition $\boldsymbol{\rho}(t) = \bar{\boldsymbol{\rho}} = [\bar{M}_a \ \bar{h}]^T$ so as to zero out the forces and moments contribution of the body and control surfaces. The EoM can be represented in a general parameter-dependent form as:

$$\begin{cases} \dot{\mathbf{x}}(t) = \mathbf{f}_x[\mathbf{x}(t), \mathbf{u}(t), \boldsymbol{\rho}(t)], \ \ t \in \Re_+ \\ \mathbf{y}(t) = \mathbf{f}_y[\mathbf{x}(t), \mathbf{u}(t), \boldsymbol{\rho}(t)] \end{cases} \tag{1}$$

where $\mathbf{x} = [p\, q\, r\, \phi\, \theta\, \psi\, V\, \alpha\, \beta\, x_L\, y_L\, z_L]^T$ represents the state vector, $\mathbf{u} = [T\, \delta_a\, \delta_e\, \delta_r]^T$ is the control input vector, and $\mathbf{y} = [n_x\, n_y\, n_z\, p\, q\, r]^T$ is the output vector. The aircraft is in equilibrium if $\dot{\mathbf{x}}(t) \triangleq 0$. Solving this condition assumes that there are as many algebraic equations as unknown variables, which is not the case. To overcome this, some of the unknown states need to be imposed. Assuming a steady wings-level flight, ϕ, p, q, and r are considered null and x_L, y_L, and ψ are specified freely. V is defined as known given its correlation with α through lift (Stevens et al., 2015). Null flight path angle is imposed as an additional constraint, assuming equal values for α and θ.

In the present study, the flight control system targets a single condition: Mach 0.5 at 5400 meters altitude, where only the longitudinal motion is relevant. Thus, from the complete linearized dynamics, the appropriate states, inputs, and outputs are selected so as to form a linear-time-invariant system with phugoid and short period (SP) eigenmotions. The pilots can easily manage the low frequency (LF) phugoid, although it still needs to meet certain damping requirements (Stevens et al., 2015). Nonetheless, the SP is pivotal for controller design and for HQ satisfaction. Thus, the following SP approximation of the Flying-V, $G_{SP}(s)$, is considered:

$$\begin{aligned} \begin{bmatrix} \dot{\alpha} \\ \dot{q} \end{bmatrix} &= \begin{bmatrix} -0.601 & 0.974 \\ -1.154 & -0.748 \end{bmatrix} \begin{bmatrix} \alpha \\ q \end{bmatrix} + \begin{bmatrix} -0.141 \\ -3.198 \end{bmatrix} \delta_e \\ \begin{bmatrix} n_{z_{IMU}} \\ q \end{bmatrix} &= \begin{bmatrix} 8.808 & -0.127 \\ 0 & 1 \end{bmatrix} \begin{bmatrix} \alpha \\ q \end{bmatrix} + \begin{bmatrix} -0.047 \\ 0 \end{bmatrix} \delta_e \end{aligned} \tag{2}$$

The open loop design model $G(s)$ is obtained by augmenting $G_{SP}(s)$ with the first order actuator model of the elevator, $G_{\delta_e}(s)$, which has a time constant of 0.07 seconds (see Figure 1).

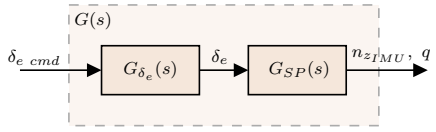

Fig. 1. Augmented open loop model, $G(s)$.

3. FLIGHT CONTROL SYSTEM DESIGN

3.1 C* Longitudinal Control Law

The C* parameter originated from a HQ criterion, which led to the creation of a response type. Variations of the C* control law became standard in the commercial aviation industry (Arent and Falatko, 1992; Favre, 1994). The parameter is defined as a normalized sum of the pitch rate q and normal acceleration at the pilot station (PS) $n_{z_{PS}}$, as described in (3):

$$C^* = n_{z_{PS}} + \frac{V_{CO}}{g} q = C^*_{PS}, \tag{3}$$

where g is the standard gravity and V_{CO} corresponds to the crossover velocity, where both cues translate into equal pilot sensation. It is asserted that pilots respond to a combination of these two signals, where the control priority shifts naturally from q to n_z as airspeed increases (Niedermeier and Lambregts, 2012).

3.2 Design Requirements

For controller design, the requirements considered are:

(R1) Disturbance rejection at plant input and outputs.
(R2) Sensor noise attenuation at plant input and outputs.
(R3) Control effort reduction.
(R4) Minimum allowable limit for the classical stability gain (GM) and phase (PM) margins of 6 dB and 45°, respectively, at plant input and outputs.
(R5) Robustness guarantees in the presence of independent parametric uncertainties in the aerodynamic coefficients, varied across the range of ±30%.
(R6) Predicted HQ within Level 1.

To achieve R6, a reference model is necessary for model matching design. The following reference model was iteratively tuned to achieve the desired dynamics for the short-term pitch response specifications (Tischler et al., 2017):

$$T_{ref}(s) = \frac{C^*_{ref}(s)}{r(s)} = \frac{K_{num}(s + z_{ref})}{s^2 + 2\xi_{ref}\omega_{ref}s + \omega^2_{ref}}, \tag{4}$$

where r corresponds to the pilot stick input signal. To minimize control surface activity (Favre, 1994), the desired natural frequency is set to ω_{ref} =1.4 rad/s, which is close to the nominal bare airframe value (ω_{SP} =1.25 rad/s) for the chosen flight condition. Additionally, defining the desired damping ratio as $\xi_{ref} = 0.75$ and the numerator $z_{ref} = 1.2$ yields Level 1 performance in the selected HQ criteria. $K_{num} = 1.6333$ was defined so that T_{ref} has an unitary static gain.

3.3 Controller Structure

The flight control law is expressed as the transfer function:

$$\delta_{e\ cmd} = K_{FB}(r - C^*_{IMU}) - K_q q \tag{5}$$

which is inspired by Niedermeier and Lambregts (2012)'s work. The parameters K_{FB} and K_q correspond to the

tunable blocks whose structure is defined a priori as an integrator times a gain and a gain, respectively. The gain K_q is applied on the pitch rate channel to improve the SP damping. The standard C* parameter is defined at the PS (see (3)), due to its strong alignment with pilot cues, making it the preferred signal for reference tracking. However, the feedback signal is C^*_{IMU} which is calculated with n_z measured at the inertial measurement unit (IMU) location. The IMU position is assumed to be near the aircraft's instantaneous center of rotation (ICR), although a more in-depth analysis must be conducted on this.

3.4 Signal-Based $\mathcal{H}_\infty$ Optimization

The final design configuration is inspired from robust control theory (Skogestad and Postlethwaite, 2005) and it is represented in Figure 2. The reference tracking and flight control system (FCS) subsystems are expanded in Figures 3 and 4, respectively. The inputs include the disturbances d_i and d_o and the sensor noise n. Additionally, the model $G(s)$ was augmented to contain the output $\dot{q}$. This parameter is used for the computation of the reference tracking signal C^*_{PS} which is dependent on $n_{z_{PS}}$ (see (6)).

$$n_{z_{PS}} = n_{z_{IMU}} + \frac{\dot{q}(x_{IMU\to CoG} + x_a)}{g_0}, \tag{6}$$

Here, the term $x_{IMU\to CoG}$ corresponds to the distance from the IMU to the center of gravity (CoG) location and x_a is equal to the distance between the CoG and the PS.

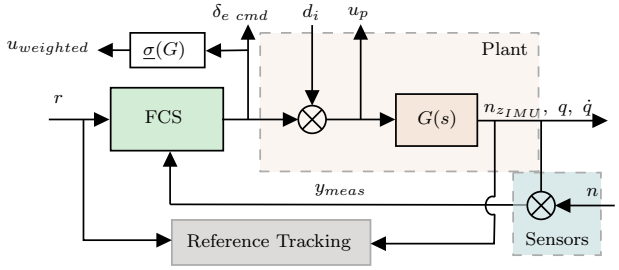

Fig. 2. Configuration for the structured controller design.

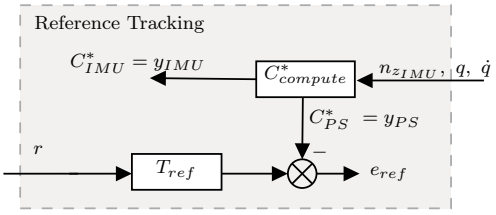

Fig. 3. Reference tracking subsystem expanded.

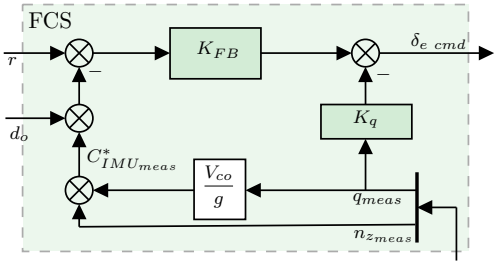

Fig. 4. FCS subsystem expanded.

Seven individual transfer functions, $C(s)$, are shaped to achieve the requirements outlined in Section 3.2, via weighting filters (WF):

(C1) $S_o(s)$ $(d_o \to y_{IMU})$ involves output disturbance rejection at the virtual plant output (PO), C^*_{IMU}. The transfer function LF gain must be reduced to enhance the rejection properties and the peak at medium frequencies (MF) should be attenuated.

(C2) $S_i(s)$ $(d_i \to u_p)$ rejects disturbances at the plant input. Similarly to S_o, small gain at LF is necessary.

(C3) $T_i(s)$ $(d_i \to \delta_{e\ cmd})$ rejects input disturbances at the controller output by having low gain at high frequencies (HF). The control signal is also attenuated.

(C4) $T_o(s)$ $(r \to y_{IMU})$ attenuates sensors noise. Thus, the transfer function from n to y_{IMU} could also be selected for the same purpose. Since noise is a HF signal, $T_o(s)$ must have low gain in this range.

(C5) $KS_o(s)$ $(d_o \to u_{c,weighted})$ reduces control effort and provides noise attenuation at HF by its low gain. For better interpretation of the attenuation level at MF and HF, the signal $u_{c,weighted}$ is used. This parameter originates from the multiplication of u with the scaling $\underline{\sigma}(G)$. This is because, at LF, the transfer function from d_o to u is approximately equal to the plant gain inverse.

(C6) $S_oG(s)$ $(d_i \to y_{IMU})$ constrains the input disturbances at the virtual PO. Small LF gain is mandatory.

(C7) $M(s)$ $(r \to e_{ref})$ is the model matching constraint that imposes the T_{ref} behavior on the signal C^*_{PS} response. It must have low gain at LF and MF.

Hence, the disturbance rejection requirement R1 is ensured by C1, C2, C3, and C6. The noise attenuation specification R2 is achieved by imposing C4 and C5, while R3, the control effort reduction, is guaranteed by C5. The stability margins, R4, result from MF peak limitation in C1. In fact, a peak in the sensitivity and complementary sensitivity functions is unavoidable (Stein, 2003) and it is related to the closest distance to the critical point -1 in the complex plane, which affects the stability margins, as described by (Seiler et al., 2020):

$$\alpha_{max} = \frac{1}{\|S + \frac{\sigma - 1}{2}\|_\infty}, \tag{7}$$

where α_{max} represents the smallest of all the frequency-dependent Disk Margins (DM) and σ represents the skew. Moreover, unstructured input and output multiplicative uncertainty is addressed by T_i and T_o. Thus, C3 and C4 contribute to R5. Lastly, C7 yields HQ compliance (R6).

The hard constraints are written as $\|W_{C_i}(s)C_i(s)\|_\infty$, where i is the index of the vector. These are a function of the WFs $W_C(s) = [W_{S_o} W_{S_i} W_{T_i} W_{T_o} W_{KS_o} W_{S_oG} W_M]^T$. Hence, the expression in (8) is verified, which concludes that defining the WF as the inverse of the desired shapes for each transfer function of $C(s)$ and having a performance level, $\gamma \leq 1$ ensures that the imposed gain limitations are satisfied.

$$\|W_{C_i}(s)C_i(s)\|_\infty < \gamma \iff \forall \omega \in \Re, |C_i(j\omega)| < \frac{\gamma}{|W_{C_i}(j\omega)|} \tag{8}$$

The WF inverse characteristics are presented in Table 1[1]. The tendency of the filters inverse for the transfer functions in C1, C2, C6, and C7 follow a similar tendency to W_1^{-1}, whereas C3, C4, and C5 are similar to W_2^{-1}, which are described in (9).

$$W_1^{-1}(s) = \frac{s + \underline{k}\overline{k}}{\overline{k}^{-1}s + \underline{k}}, W_2^{-1}(s) = \frac{\overline{k}s + \underline{k}}{s + \overline{k}\underline{k}^{-1}}, \quad (9)$$

where $\underline{k}$ and $\overline{k}$ correspond to the LF and HF attenuation, respectively, and $\underline{\overline{k}}$ is a certain attenuation at frequency $\underline{\overline{\omega}}$.

Table 1. Weighting filters characteristics.

	$W_{S_o}^{-1}$	$W_{S_i}^{-1}$	$W_{T_i}^{-1}$	$W_{T_o}^{-1}$	$W_{KS_o}^{-1}$	$W_{S_oG}^{-1}$	W_M^{-1}
$\underline{k}$ (dB)	-50	-50	12.04	12.04	50	-50	-50
$\underline{\overline{\omega}}$ (rad/s)	1.70	4.60	7.96	3.08	14.30	10^{-2}	1
$\underline{\overline{k}}$ (dB)	0	0	0	0	-4.80	-25.30	-20.9
$\overline{k}$ (dB)	5.58	5.58	-80	-80	-50	30	-10
Order	1	1	2	2	1	1	1

These design specifications are defined via `sltuner()`[2] which interfaces with a Simulink® file that mimics the configuration in Figure 2. For each constraint, the obtained γ is displayed in Table 2. The controllers retrieved are shown in (10), whose orders are based on an a-priori unstructured synthesis step.

$$K_{FB} = \frac{-0.20696}{s} \qquad K_q = -1.43320, \quad (10)$$

Table 2. γ values obtained for each constraint.

	S_o	S_i	T_i	T_o	KS_o	S_oG	M
γ	0.9996	0.9998	0.9998	0.9587	0.9968	0.9935	0.9965

The frequency responses of the closed loops transfer functions S_o and T_o, S_i and T_i, KS_o, S_oG, and M are shown in Figures 5, 6, 7, 8, and 9, respectively, as well as the corresponding WF inverse. A feedforward controller is often used to improve the reference tracking performance. However, it is verified that the controller is not necessary in the current design, which is explained by Figure 10. The ideal feedforward controller $K_{FF_{ideal}} = T_{o_M}^{-1} \cdot T_{ref}$, where T_{o_M} is the transfer function from r to C_{PS}^*. The most dominant pole and zeros of $T_{o_M}^{-1}$ have frequencies of $\omega_p = 1.4$ rad/s and $\omega_z = 1.82$ rad/s, respectively, while T_{ref} has poles and a zero with frequencies of $\omega_p = 1.4$ rad/s and $\omega_z = 1.2$ rad/, respectively. The frequencies proximity suggests that T_{o_M} has an approximate behavior to the desired T_{ref}, highlighting the feedforward controller as noncompulsory. This statement is to be corroborated by the HQ and nonlinear simulations analysis.

The open loops singular values at the plant input, Li, and at the PO at $n_{z_{CoG}}$ and q, respectively Lo_{n_z} and Lo_q, and at the virtual PO C_{IMU}^*, $Lo_{C_{IMU}^*}$, are shown in Figure 11. On the one hand, the LF small gain in the sensitivity functions are translated into large gains in the open loops at the plant input and virtual PO. On the other hand, T_o and T_i impose roll off in the open loops at HF. Nevertheless, the lack of disturbance rejection on n_z and q is verified, given the small gain at LF. Such

[1] `makeweight()` MATLAB® function is used to obtain the WF..
[2] The `TuningGoal.Gain` class is used to impose the gain limits from a specified input to a specified output over the frequency range.

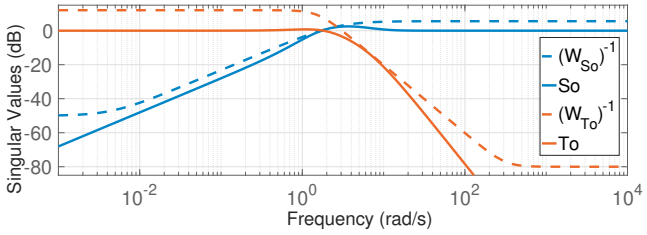

Fig. 5. Frequency responses of $S_o(s)$ and $T_o(s)$.

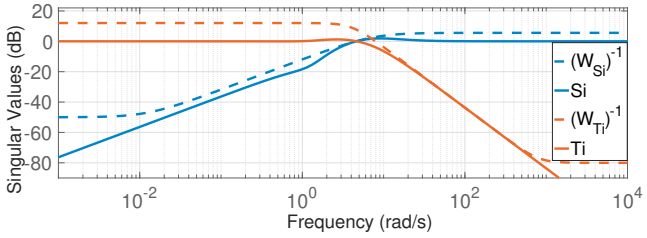

Fig. 6. Frequency responses of $S_i(s)$ and $T_i(s)$.

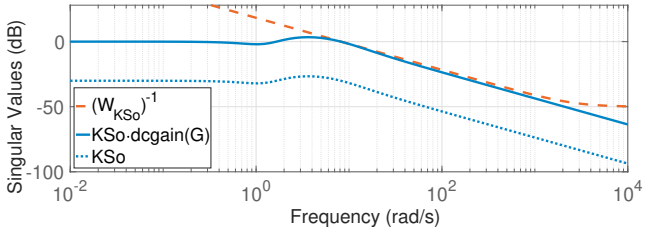

Fig. 7. Frequency response of $KS_o(s)$.

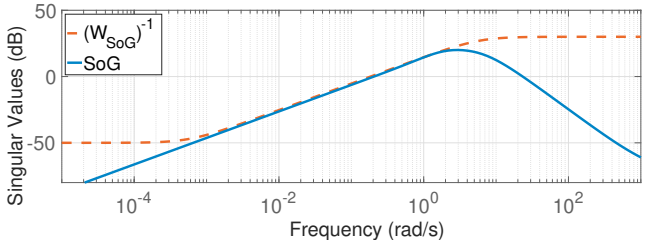

Fig. 8. Frequency response of $S_oG(s)$.

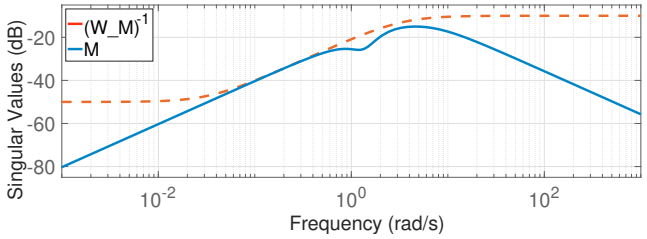

Fig. 9. Frequency response of $M(s)$.

outcome is expected since no integral action is applied on these signals. Additionally, since the plant has only one singular value, it is not possible to control more than one output with one input. Thus, it is concluded that to have a balanced disturbance rejection at LF on n_z and q, the pure C* configuration should be followed, which also yields good disturbance rejection in this signal. If integral action is applied on the n_z (or q) signal, the q (or n_z) disturbance rejection is aggravated, with smaller gain observed at LF.

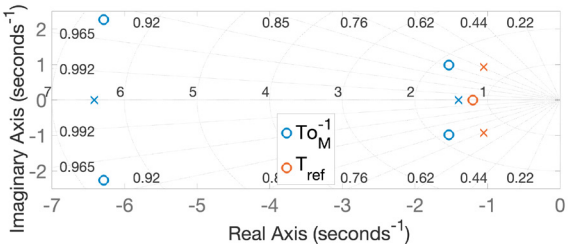

Fig. 10. r to C^*_{PS} transfer function and T_{ref} pzmap.

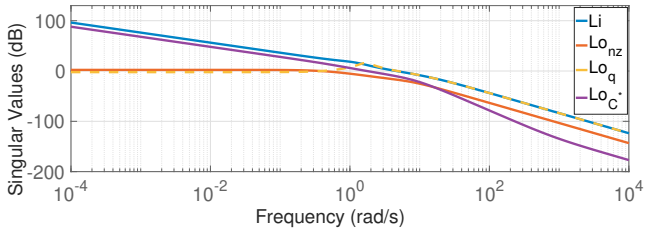

Fig. 11. Open loops frequency response at the plant input and output.

4. FLIGHT CONTROL SYSTEM ANALYSIS

4.1 Stability Margins

Stability margins (SM) assessment is a key specification, as highlighted by R4, which is also crucial when uncertainty is applied to the system (R5). Anonymous (2008) states that in the latter scenario, the requested SM are reduced, highlighting an allowable degradation up to 50% of the desired nominal values if faced by ±20% uncertainty. In this study, parametric uncertainty bounded by ±30° is applied to the stability and control derivatives that affect the SP the most (i.e. C_{z_α}, C_{m_α}, C_{m_q}, and $C_{m_{\delta_e}}$). Five uniformly distributed samples were taken in this range for each coefficient, yielding 625 uncertain conditions. Therefore, the classical loop-at-a-time SM are computed, as well as the balanced (S-T) Disk Gain and Phase Margins (DGM and DPM, respectively). Table 3 presents these values for the nominal scenario, whereas Table 4 shows the worst case (WC) results for the uncertainty simulations. It is verified that the minimum values of 6 dB and 45° of GM and PM, respectively, are guaranteed for the nominal system and uncertainty scenarios.

Table 3. Disk (S-T) and classical loop-at-a-time GM and PM, for the nominal scenario.

	Disk Margins		Classical Margins	
Broken Loop	DGM (dB)	DPM (°)	GM (dB)	PM (°)
Plant Input	± 11.19	± 59.16	∞	59.65
PO ($n_{z_{CoG}}$)	± 12.84	± 64.31	14.54	127.02
PO (q)	± 10.94	± 58.32	-15.40	58.36
Virtual PO (C^*_{IMU})	± 10.38	± 56.32	18.63	59.02

Table 4. WC disk (S-T) and classical loop-at-a-time GM and PM, subject to uncertainty.

	Disk Margins		Classical Margins	
Broken Loop	DGM (dB)	DPM (°)	GM (dB)	PM (°)
Plant Input	± 9.00	± 50.92	∞	55.69
PO ($n_{z_{CoG}}$)	± 9.60	± 53.36	10.77	119.59
PO (q)	± 8.31	± 47.99	-28.47	51.27
Virtual PO (C^*_{IMU})	± 7.14	± 42.55	14.59	45.98

4.2 Handling Qualities

Handling qualities represent the dynamic characteristics of an aircraft as perceived by the pilot, which highly influence the safety, performance, and pilot workload. Thus, analyzing HQ criteria is crucial to ensure the aircraft responds predictably and effectively. Three main criteria are used, namely the attitude bandwidth (BW), the flight path BW, and the pitch rate overshoot & pitch attitude dropback, as proposed by Mitchell et al. (1994). The results are shown in Figures 12, 13, and 14, respectively. The BW is calculated as the highest frequency at which the PM is at least 45° and the GM is at least 6 dB. Considering w_{180} as the frequency at which the phase crosses -180°, the phase delay parameter τ_p is computed by dividing the difference in phase from ω_{180} to $2\omega_{180}$ with the frequency $2\omega_{180}$, with appropriate scaling with units. Secondly, the flight path bandwidth, ω_{BW_γ}, is defined as the frequency at which the response of γ lags the cockpit control input by 135°. Lastly, the subscript in q_{ss} signifies steady state. Besides the nominal values, the ones retrieved from the 625 uncertain conditions are also shown. As desired, the nominal case is within Level 1 and the uncertain points are also mostly within this level, except for some outliers.

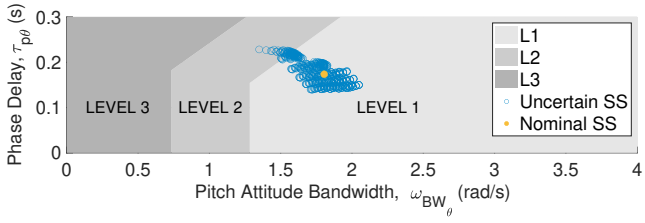

Fig. 12. Pitch attitude BW HQ criteria.

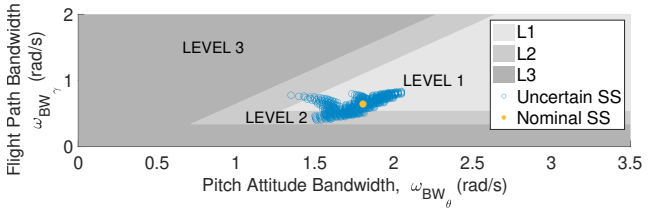

Fig. 13. Flight path BW HQ criteria.

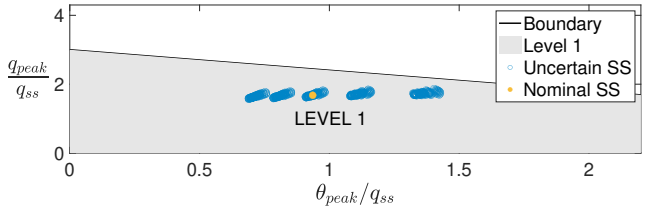

Fig. 14. Pitch rate overshoot & attitude dropback HQ criteria.

4.3 Nonlinear Time Domain Simulations

The linear controller is implemented in the nonlinear 6 DoF model. The reference tracking signal is shown in Figure 15, while Figure 16 shows the corresponding control surface deflections. Lastly, Figure 17 shows the performance signal when input and output disturbances with amplitudes of 2° and -3° and 0.3 and -0.2, respectively, are introduced.

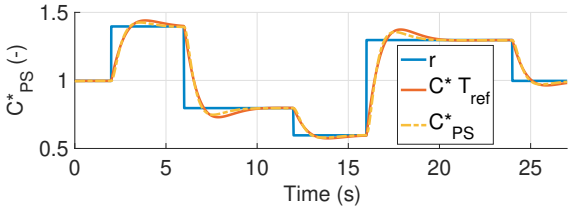

Fig. 15. Reference tracking C^*_{PS} response.

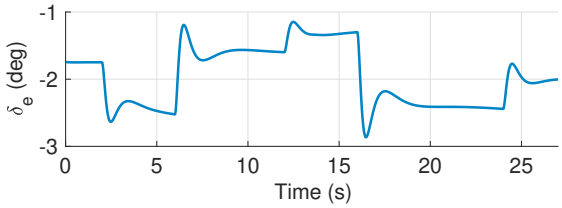

Fig. 16. Control deflection δ_e response.

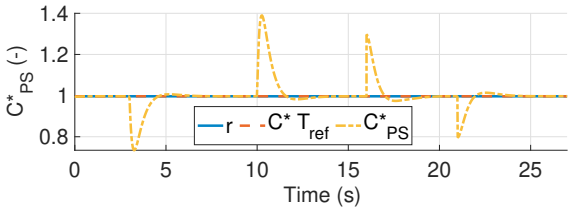

Fig. 17. C^*_{PS} response with disturbances introduced.

5. CONCLUSION

This study presented a longitudinal control law design for the Flying-V aircraft, based on a structured $\mathcal{H}_\infty$ robust control framework. The resulting controller satisfied all imposed requirements, demonstrating adequate stability margins, compliance with Level 1 handling qualities, and strong performance when evaluated on the nonlinear model. By implementing a systematic and transparent design, this research contributes to establishing a practical control benchmark for the Flying-V. Opposed to the structurally constrained methods that were previously applied on the concept aircraft, the proposed approach offers a scalable solution that explicitly addresses robustness specifications a-priori. Future work should address the discretization effects of the flight computer, expansion to lateral-directional design, and gain-scheduling to cover a larger flight envelope.

REFERENCES

Anonymous (2008). *Aerospace - Flight Control Systems - General Specification for Design, Installation, and Test of Piloted Military Aircraft. SAE-AS94900.*

Apkarian, P. and Noll, D. (2006). Nonsmooth $\mathcal{H}_\infty$ Synthesis. *IEEE Transactions on Automatic Control*, 51(1), 71–86. doi:10.1109/TAC.2005.860290.

Arent, L. and Falatko, J. (1992). 757 Fly-by-Wire Demonstrator Flight Test. In *The Boeing Company. 6th AIAA Biennial Flight Test Conference. Hilton Head, SC*, 4099. doi:10.2514/6.1992-4099.

Atmaca, D. and Kampen, E.J.V. (2025). Fault Tolerant Control for the Flying-V Using Adaptive Incremental Nonlinear Dynamic Inversion. In *AIAA SCITECH 2025 Forum. AIAA 2025-0081. American Institute of Aeronautics and Astronautics. Orlando, FL.* doi:10.2514/6.2025-0081.

Benad, J. and Vos, R. (2022). Design of a Flying V Subsonic Transport. In *33rd Congress of the International Council of the Aeronautical Sciences, ICAS 2022, Stockholm, Sweden.* URL `https://resolver.tudelft.nl/uuid:95ea413d-d5b1-4cb2-a650-828cb106dbbd`.

Doyle, J., Glover, K., Khargonekar, P., and Francis, B. (1988). State-Space Solutions to Standard $\mathcal{H}_2$ and $\mathcal{H}_\infty$ Control Problems. In *1988 American Control Conference. Atlanta, GA, USA*, 1691–1696. doi:10.23919/ACC.1988.4789992.

Favre, C. (1994). Fly-by-Wire for Commercial Aircraft: the Airbus Experience. *International Journal of Control*, 59(1), 139–157. doi:10.1080/00207179408923072.

Gahinet, P. and Apkarian, P. (1994). A Linear Matrix Inequality Approach to $\mathcal{H}_\infty$ Control. *International Journal of Robust Nonlinear Control*, 4(4), 421–448. doi:10.1002/rnc.4590040403.

Mitchell, D.G., Hoh, R.H., Aponso, B.L., and Klyde, D.H. (1994). Proposed Incorporation of Mission-Oriented Flying Qualities into MIL-STD-1797A. WL-TR-94-3162. *Wright-Patterson AFB, USA.*

Niedermeier, D. and Lambregts, A. (2012). Fly-by-Wire Augmented Manual Control - Basic Design Considerations. *ICAS 2012-5.4.1. 28th Congress of the International Council of the Aeronautical Sciences 2012, ICAS 2012. Brisbane, Australia*, 4, 3073–3086.

Seiler, P., Packard, A., and Gahinet, P. (2020). An Introduction To Disk Margins. *IEEE Control Systems Magazine*, 40.

Skogestad, S. and Postlethwaite, I. (2005). *Multivariable Feedback Control: Analysis and Design*, volume 2. John Wiley and Sons.

Stein, G. (2003). Respect the Unstable. *IEEE Control Systems Magazine*, 23(4), 12–25. doi:10.1109/MCS.2003.1213600.

Stevens, B.L., Lewis, F.L., and Johnson, E.N. (2015). *Aircraft Control and Simulation: Dynamics, Controls Design, and Autonomous Systems.* ISBN: 978-1118870976. John Wiley & Sons. doi:10.1002/9781119174882.

Stougie, J., Pollack, T., and Van Kampen, E.J. (2024). Incremental Nonlinear Dynamic Inversion control with Flight Envelope Protection for the Flying-V. In *AIAA SCITECH 2024 Forum. AIAA 2024-2565. American Institute of Aeronautics and Astronautics. Orlando, FL*, 2565. doi:10.2514/6.2024-2565.

Tischler, M.B., Berger, T., Ivler, C.M., Mansur, M.H., Cheung, K.K., and Soong, J.Y. (2017). *Practical Methods for Aircraft and Rotorcraft Flight Control Design: An Optimization-Based Approach.* ISBN: 978-1624104435. American Institute of Aeronautics and Astronautics.

van Overeem, S., Wang, X., and Van Kampen, E.J. (2023). Handling Quality Improvements for the Flying-V Aircraft using Incremental Nonlinear Dynamic Inversion. In *AIAA SCITECH 2023 Forum. AIAA 2023-0105. American Institute of Aeronautics and Astronautics. National Harbor, MD Online*, 0105. doi:10.2514/6.2023-0105.

Zipfel, P.H. (2007). *Modeling and Simulation of Aerospace Vehicle Dynamics.* AIAA: American Institute of Aeronautics and Astronautics, Inc., 2nd edition.